Theoretical and experimental investigations of different area ratios of a supersonic ejector driven by compressed air

Ahmed AL-nuaimi[1,†], Mark Worall[2] and Saffa Riffat[3]
[1]*Faculty of Engineering, University of Nottingham, Nottingham NG7 2RD, UK;* [2]*Faculty of Engineering, University of Nottingham, Nottingham NG7 2RD, UK;* [3]*Faculty of Engineering, University of Nottingham, Nottingham NG7 2RD, UK;*

Abstract

Ejectors have some advantages such as being simple, reliable and no moving parts. They can be used in air-conditioning and refrigeration applications. This paper presents a comparison of ejector performance, primary pressure (*Pp*), back pressure (*Pb*) and area ratios of ejectors (A_2/A_t) predictions by an analytical model and a computational fluid dynamics model for different operating conditions. Six different area ratios of ejector using air as working fluid in this study were proposed and tested experimentally. The variable area ratios of ejectors (A_2/A_t) were used with a range from 10.68 to 30.62. Two sets of ejectors (A and C) are studied and examined depend on the kind of nozzle. The aim of this study was to investigate these ejectors under variation of primary pressure (*Pp*) (1.5–6.0 bar) and adjustable spindle position (0 to −25 mm). Two groups of ejectors (A and C) were categorized based on the type of nozzle. The experimental results validate the solutions of the main parameters of ejectors using air as working fluid. The results show that group A is more appropriate for higher values of back pressure, while group C is more suitable for high performance of the ejector. Finally, the main parameters were carried out on six different ejectors to find the best combination based on various nozzles and constant area sections.

Keywords: Ejector; Air-conditioning and refrigeration; Entrainment ratio; Adjustable spindle ejector; Variable area ratios

Corresponding author.
ahmed_i1974@yahoo.com

Received 31 March 2019; revised 25 June 2019; accepted 18 July 2019

1 INTRODUCTION

Ejectors have been used in cooling systems since the 1900s [1]. They were not preferred in refrigeration systems because of their low coefficient of performance (COP). However, ejectors have some advantages such as being simple, reliable, with no moving parts. Moreover, several heat sources using these devices. For instance, waste heat, solar energy, geothermal energy and biomass products applied to drive a refrigeration system or to generate electricity. Furthermore, they reduce pollution in comparison with fossil fuel power plants. Many studies have presented various types of working fluids in ejectors. Varga *et al.* [2] and Chandra and Ahmed [3] studied water as a working fluid. R236fa, R152a and R600a were studied by Varga *et al.* [4], Zhang *et al.* [5] and Zhang *et al.* [6]. In addition, R245fa and R134a were tested by Lin *et al.* [7], Yen *et al.* [8], Lin *et al.* [9] and Hou *et al.* [10]. Moreover, two empirical correlations were derived to predict the performance of 15 ejectors using R141a [11]. Furthermore, Kumar *et al.* [12], Hemidi *et al.* [13, 14] and Mazzelli *et al.* [15] have used air in a supersonic ejector.

Many studies have been presented to study the ejector's parameters in terms of geometry, operating condition, effects of *Pb* and spindle positions on the entrainment ratio (ω). The geometry of the ejector has a significant influence on the performance of the ejector. Many studies have studied this factor to obtain a good geometry with high performance. Zhang *et al.* [5] investigated numerically and proved experimentally the effects of ejector geometry such as nozzle outlet angle, the distance between nozzle exit to the mixing chamber and the length of the diffuser section on the flow features and ω. The constant rate of momentum change was initially proposed by Eames [16] and developed by incorporating friction effects by Kumar *et al.* [12]. Varga *et al.* [2] discussed a variable geometry ejector experimentally and numerically in a 5 kW ejector air-

[†]Ahmed AL-nuaimi, http://orcid.org/0000-0002-4286-6596
International Journal of Low-Carbon Technologies 2019, 14, 550–560

doi:10.1093/ijlct/ctz050 Advance Access publication 14 October 2019

conditioning system driven by solar energy. The results showed primary flow rate was in good agreement between computational fluid dynamics (CFD) and experiment under all operating conditions and spindle positions. Furthermore, the constant-area and variable-area ejectors were compared in terms of CFD and experiments at the same operating conditions. These two types of ejectors were tested in a steam jet refrigeration system. The results show that the variable area ejector increases the pressure lift ratio up to 40% by eliminating a shock wave from the ejector. The COP for variable area ejector fluctuates because the secondary flow does not attain sonic conditions [3].

The geometry effects have been mentioned above; Chandra and Ahmed [3] studied the effects of the operating conditions on ω, where ω decreases when generator temperature (T) increases from 90 to 120°C. Moreover, when the evaporator temperature increases at the same generator temperature, ω decreases. Hou *et al.* [10] used an adjustable ejector in a parallel hybrid ejector-based refrigerator–freezer cooling cycle, the authors showed that under Pp = 243.34 kpa, secondary pressure (Ps) = 84.38 kpa and Pb = 97.03 kpa, The Pb has an important influence on the performance of the ejector, ω decreases from 1.79 to 0 0.86 when the blocking percentage is 10%. The authors investigated the effect of pressure recovery ratio (PRR) in the refrigeration system, as the PRR increases and the blocking area in adjustable ejector increases to 40% (spindle moves forward), the ω has the highest value (over 2.5) but it is difficult to maintain this value and it sharply tends to zero [7]. Several studies concluded that as the spindle position moves towards the nozzle, the ω decreases, [6, 10]. Furthermore, an adjustable ejector was investigated to meet variable cooling loads in an ejector in the multi-evaporator refrigeration system, so, by adjusting the spindle position it is possible to control the primary flow rate and consequently obtain good stability in the system [7].

CFD analytical studies with different procedures have been applied to show a good agreement with experimental tests on various types of ejectors. As for turbulence models, standard k–ε model, renormalization-group k–ε model and k–ω–sst model were used in an adjustable ejector [9]. Seven turbulence models in Reynolds Averaged Navier–Stokes have been studied to find the best agreement with experimental studies. The results showed that the k–ω–sst has the best agreement amongst models with the experimental measurements concerning both global and local flow quantities [17]. To solve the coupled pressure and velocity (V) equations, the SIMPLEC algorithm was used by Lin *et al.* [9]. A comparison between experimental and theoretical (CFD) results was presented on a supersonic air ejector. For off-design predictions, two turbulence models (k–ε and k–ω–sst) were used to compare their results with experiments. k–ε showed a good agreement with the experimental result as compared with less agreement being obtained from k–ω–sst. These two models showed an issue through no matching results related to the ω under a range of operating conditions [13]. The same authors presented the CFD of a wide range of operations of a supersonic air ejector to investigate an issue in the previous study. The findings showed that a good result for the entrainment ratio does not mean a clear matching with local flow properties. For this point, both the sonic line and Mach number (M) were proposed as a key factor to explain the relationship between entrainment ratio and local flow properties. Finally, this key helps to assign the place of the critical section where the ejector become choked [14]. However, there is no base to assign the best agreement amongst the turbulence models for the ejector design.

Table 1. *Isentropic efficiencies.*

Loss coefficient	Value	References
Nozzle throat (η_n)	0.95	[20],
Nozzle exit (η_{py})	0.88	[21]
Mixing chamber (η_s)	0.85	[22]
Mixing section (η_m)	0.80	([23])
Diffuser section (η_d)	0.95	[20], [21]

The literature review above indicates that there are many studies on the ejectors theoretically and experimentally. However, few studies have been conducted by changing the primary nozzle cross-sectional area with an adjustable spindle. The aim of this paper is to investigate six different types of ejectors under variation of adjustable spindle position, primary and back pressures. According to the nozzle and constant-area section, two nozzles and three different constant-area sections were carried out in this study. In the present study, the working fluid is air to test six different ejectors. Furthermore, adjustable spindle position ranged between 0 (fully closed) when the spindle head is positioned at the outlet of the primary nozzle, and − 25 mm (fully open to change mass flow rate in inlet primary).

2 ANALYTICAL MODELLING

In ejector studies, many researchers presented a model in terms of one dimension. Keenan *et al.* [18] presented the first model of 1D ejector analysis (one-dimensional), and model modified by Eames *et al.* [19]. In the present study, air as a working fluid behaves as a perfect gas and the figure shows the flow chart of the processes used. Table 1 shows the isentropic efficiencies used in this model based on previous studies. Several assumptions are included in this analytical model:

- The primary and secondary flows are expanded from stagnation conditions.
- Steady state and adiabatic conditions are applied [13].
- The governing equations (quantity, momentum and energy) are applied from inlet to outlet [24].
- Neglect primary and secondary velocities in stagnation conditions.

As mentioned above, the isentropic efficiencies are shown in Table 1. The procedures for the calculation of the flow chart of the 1D model used in this study is shown in Figure 1. Furthermore, the operating conditions were applied in this investigation as follows: Pp (1.5–6.0 bar), Pb (0.5–0.8 bar) and secondary pressure (Ps) (0.1–0.37 bar), as well as the ambient temperature (300 K), for all types of ejectors.

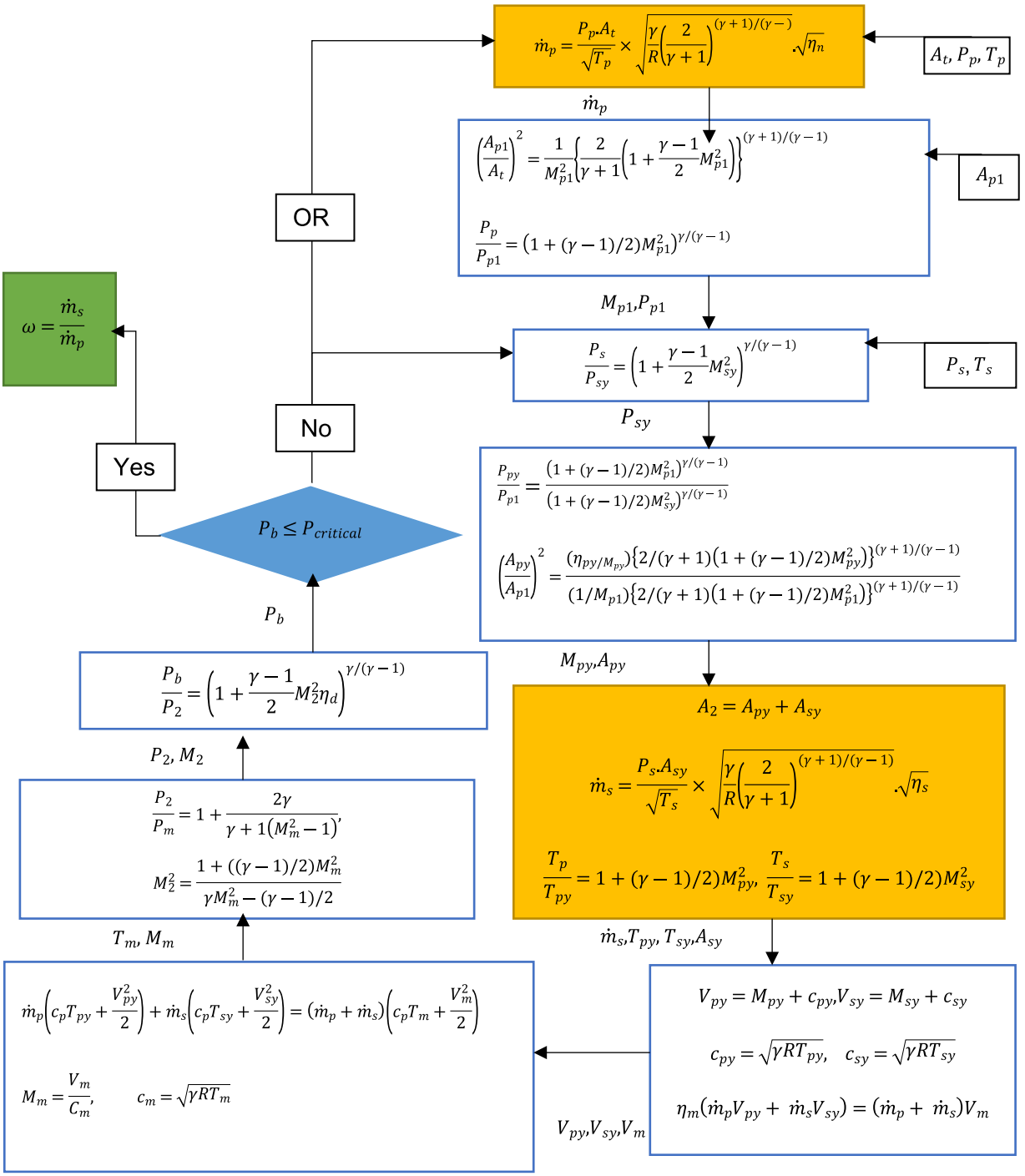

Figure 1. *Calculation of flow chart of 1-D model.*

3 CFD MODELLING

A computational study to test six types of ejectors was carried out using Fluent 18.1. A control volume using discretization method was used to solve by the Navier-–Stokes equations. While, 2D axis-symmetric system was applied to solve the computational domain. The axisymmetric system is applied to the models of the six types of ejector in a 2D domain as shown in Figure 2. The geometries of the ejectors are specified in Figure 5, Table 3 and Table 4. The grids of ejector models are included in Table 2 for all types of ejectors. It is obvious that the concentrated grids are found in the main important regions showing high changes in flow. For links between pressure and velocity, a semi-implicit procedure for pressure-linked equations (SIMPLE) algorithm was used to solve

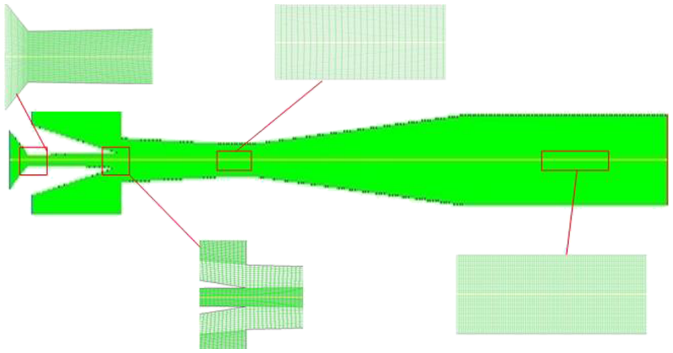

Figure 2. *Grid structure of the ejector model.*

Table 2. *Number of mesh cells.*

Type	Number of mesh cells	Type	Number of mesh cells
AA	18070	CA	20504
AB	16659	CB	19351
AC	17955	CC	20436

the discretized equations for air as compressible flow. A second-order upwind scheme for interpolation employing a mesh ranging from coarser to finer and selected mesh is shown in Table 2 with structured quadrilateral mesh cells was carried out.

In this study, k–ω was the turbulence model selected to obtain more accurate results and good agreement with findings from analytical and experimental approaches. The turbulence intensity and viscosity ratio were taken as 5% and 10, respectively. Moreover, the time option was set in steady. The boundary conditions of ejectors in terms of primary and secondary inlets were specified as 'pressure inlet', and the 'pressure outlet' was applied for the discharge. The working fluid in the CFD modelling is air. Its density is assumed as ideal gas behaviour. Other thermodynamic properties such as specific heat, thermal conductivity, viscosity and molecular weight are obtained from the EES software.

The result is obtained when the iterations continued until the residual for governing equation arrives below 10^{-5} to confirm that convergence is reached. It is found that the residual for continuity equation is below 10^{-5} while the residuals for other equations such as the energy equation, the momentum equation and the turbulent kinetic energy are below 10^{-7}.

4 EXPERIMENTAL INVESTIGATIONS

4.1 Description of the test rig

A schematic of the ejector diagram is shown in Figure 3. The working principle and operating procedure of the system is described below:

- The rig consists of two main components (compressor and ejector) connected by copper and nylon pipes as well as joints such as valves, flow meters, filter, oil level and other measurements devices.

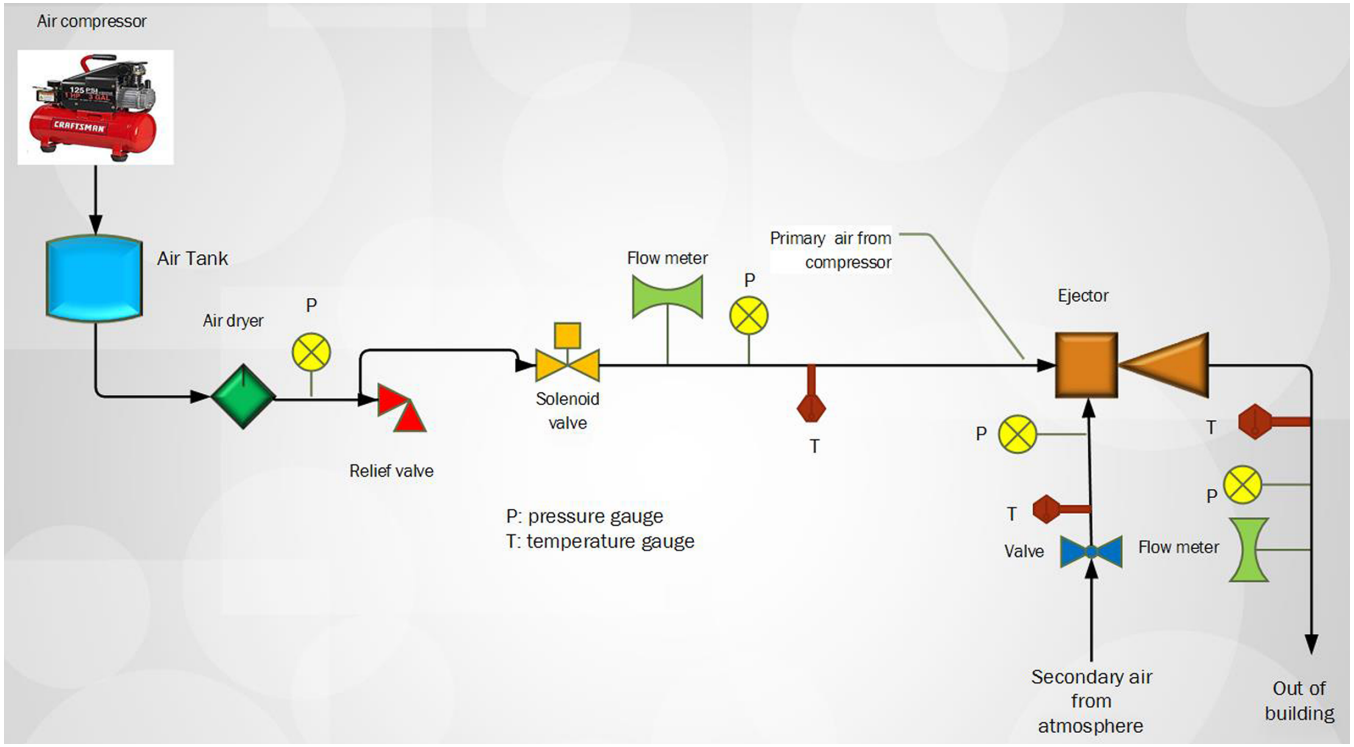

Figure 3. *A simple circuit diagram of the ejector cycle.*

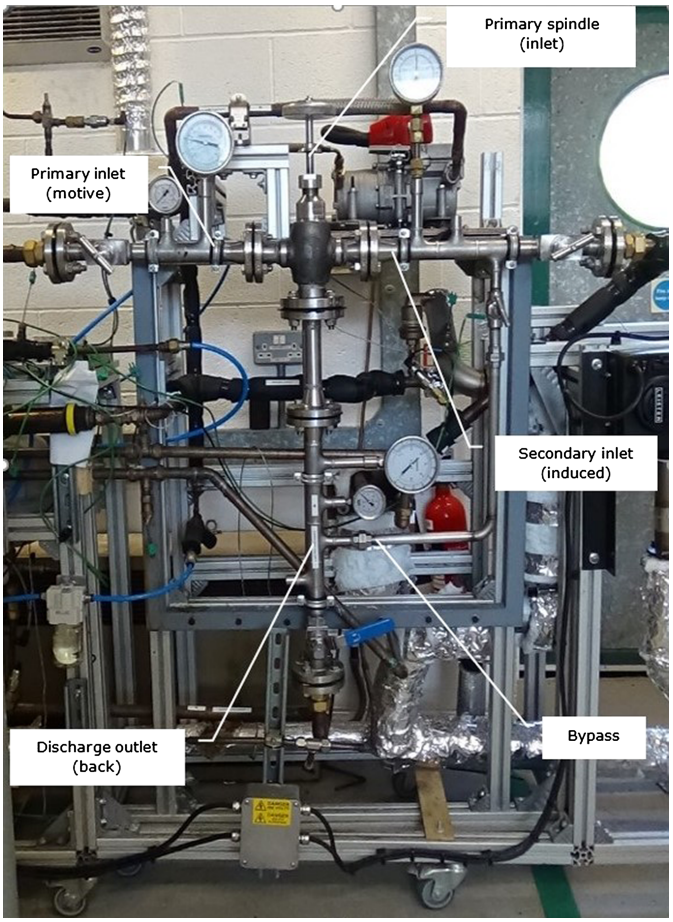

Figure 4. *Experimental setup of the rig.*

- Figure 3 shows a simple circuit diagram of the ejector cycle. Air is compressed from an air supply source in the lab to the main line before the relief valve.
- In this cycle, the air is supplied to a nozzle in the ejector at high pressure (*Pp*) to expand to the pressure of the surroundings, this will release the air flow from the low-pressure side (suction pressure).
- Both streams are mixed and recompressed to the exhaust line to the atmospheric environment. Figure 4 shows the experimental setup of the rig.

Several instrumentations and sensors were installed in this rig to measure temperature, pressure and flow rates in primary, secondary and discharge ports. The pressure transmitter PT5-30 M (pressure range: 0–30 bar) and PT5-7 M (pressure range: −0.08–7 bar) with an accuracy of 1% were used to measure inlet and outlet pressures. Temperatures were measured with a K-type thermocouple (model RS No. 397-1488) with an accuracy of ±1.5°C and range 0–1100°C. Furthermore, flow meters (model RMC) with an accuracy of 2% were installed to read the flow rates in the inlets and outlet.

In the present study, six fixed different variable area ratios of ejector were used to validate analytical and CFD results experimentally. Variable area ratios of ejectors (A_2/A_t) and their parts are shown in Figure 5.

This figure represents the main parts of the ejector such as a nozzle, three types of constant-area sections (including discharge) and an adjustable spindle of the primary inlet that ranges from 0 (fully closed) to −25 mm (fully open). Moreover, it shows two separate internal sets of nozzles (A), and (C) with an adjustable spindle that allows varying of the primary mass flow. The motive, suction and discharge connections are 1' ASME B16.5 150 lb WN flanges and for easy changing of constant-area sections. These parts are designed and fabricated to use in the experimental tests. The six ejectors of the experimental test were manufactured by Venturi Jet Pumps Ltd. (Stoke on Trent, UK).

The two types of nozzles (A) and (C) were designed and manufactured for the testing. Specifications of the nozzles are detailed in Table 3. The three types of constant-area sections are listed in Table 4. Six different area ratios (A_2/A_t) of ejectors are tested in this experiment and they range from 10.68 to 30.62. For simplicity, the ejector AB refers to the ejector that includes the type of nozzle A and type of constant-area section B.

4.2 Test procedure

Experimental tests were carried out under a range of *Pp* from 1.5 to 6.0 bar and ambient temperature. Through the individual test of ejectors, monitoring was carried out by matching the pressure gauge of primary and value from data taker (D80) under small increments in *Pp* (0.5 bar each step). Logging was carried out over data received from D80 for inlet secondary and outlet discharge (back) pressures under each *Pp* point. In addition, flow rates for all inlets and outlet were measured manually by a flow meter device (flow meter RMC). In this work, ω and area ratio A_r are the main dimensionless parameters used. These parameters can be expressed by the following equations:

Equation 1: Entrainment ratio of the ejector.

$$\omega = \frac{\dot{m}_s}{\dot{m}_p},$$

where

- $\dot{m}_p$ = mass flow rate of inlet primary (kg/s)
- $\dot{m}_s$ = mass flow rate of inlet secondary (kg/s).

Equation 2: Area ratio of the ejector.

$$A_r = \frac{A_2}{A_\tau},$$

where

- A_2 = constant-area section (m^2)
- A_t = throat nozzle area (m^2).

The ejector operates at subsonic mode at the diffuser section when the back pressure is higher than the critical back pressure. In this case, the ejector has no shock wave in this section due to

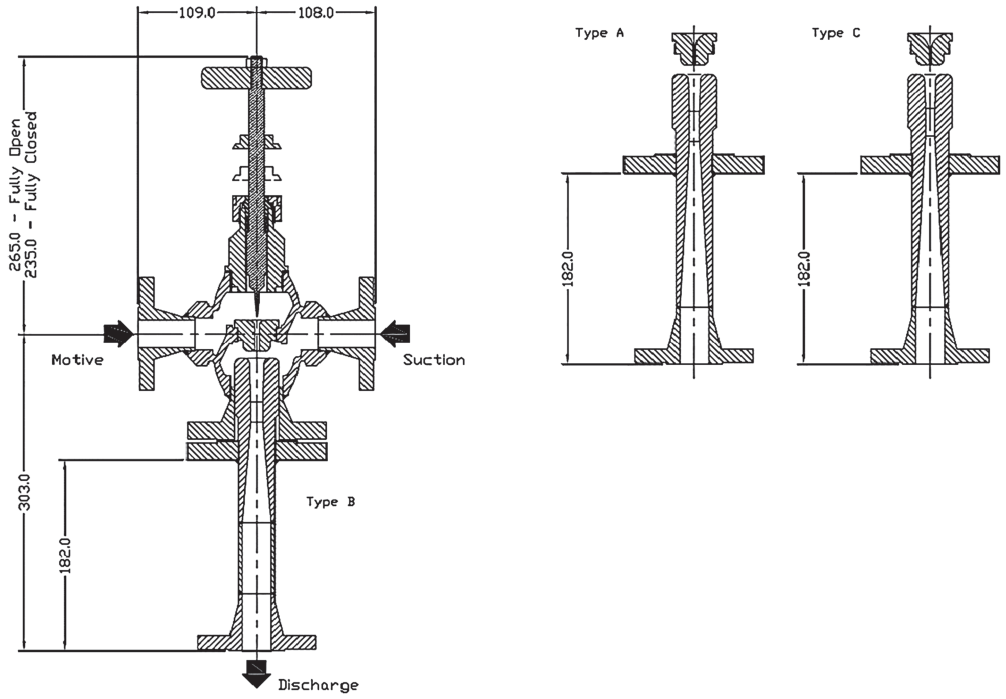

Figure 5. *Diagram of ejector design.*

Table 3. *Specifications of the nozzles.*

Nozzle	Throat diameter, dt (mm)	Exit diameter, dpl (mm)	Apl/At
A	2.60	3.22	1.53
C	1.93	2.0	1.55

increased pressure. In the case of the critical mode, the ejector works at optimum conditions when the back pressure is lower than critical back pressure and the stronger shock wave happens in this case and after nozzle exit. These behaviours are shown in Figures 6 and 7, whereas the relation between pressure and velocity is indirect. The primary pressure and secondary pressure are high at the beginning and the velocity is subsonic.

The primary pressure enters the nozzle at very high pressure and faces chocking at the throat of the nozzle and decreases in its value until lower than the secondary pressure. This creates a lower pressure zone and an increase in velocity to supersonic and allows the secondary flow to enter from the mixing chamber.

Figure 8 shows the effects of critical back pressure on the entrainment ratio for six different types of ejector based on CFD analysis. This figure shows the effect of variation of *Pb* on ω under a range of *Pp* (4.5 bar). It shows that the highest value belongs to the ejector CB at about 0.46 while the lowest value is 0.38 for ejector AC. In addition, it can be shown that the highest back pressure belongs to the ejector AC at about 0.55 bar while the lowest value is 0.19 bar for the ejector CB.

5 RESULTS AND DISCUSSION

The main parameters in this test are *Pp* at the inlet of the nozzle, *Ps* at the inlet of the suction chamber and *Pb* out of the diffuser port. The experimental results were used to investigate the effects of main parameters, A_r and adjustable spindle position on the performance of each type of ejector (ω). A comprehensive analysis of the CFD modelling, analytical and experimental results for the six types of ejectors was carried out. First, the CFD results using Fluent were verified against analytical results from EES software programme.

Table 4. *Types of ejector model.*

Constant-area section		Ejector specification			
Serial no.	Diameter(mm)	A_2/A_t (with nozzle A)		A_2/A_t (with nozzle C)	
A	9.08	10.68	AC	19.39	CC
B	10.68	12.19	AA	22.13	CA
C	8.60	16.87	AB	30.62	CB

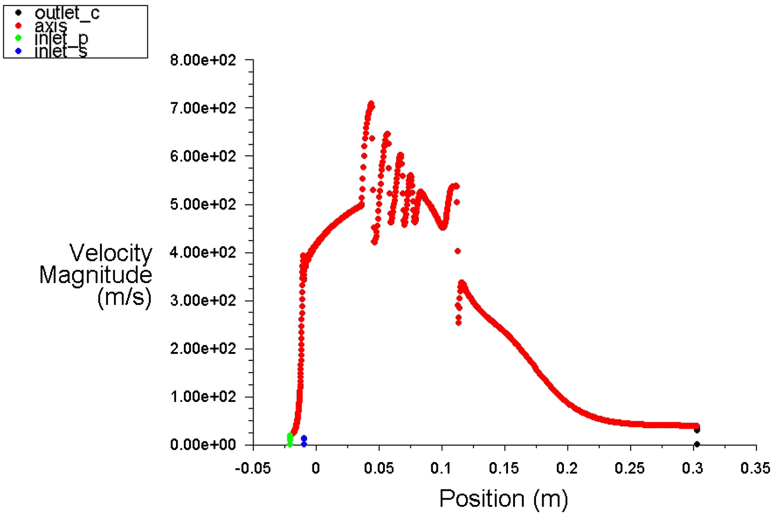

Figure 6. *Velocity magnitude along the length of the ejector.*

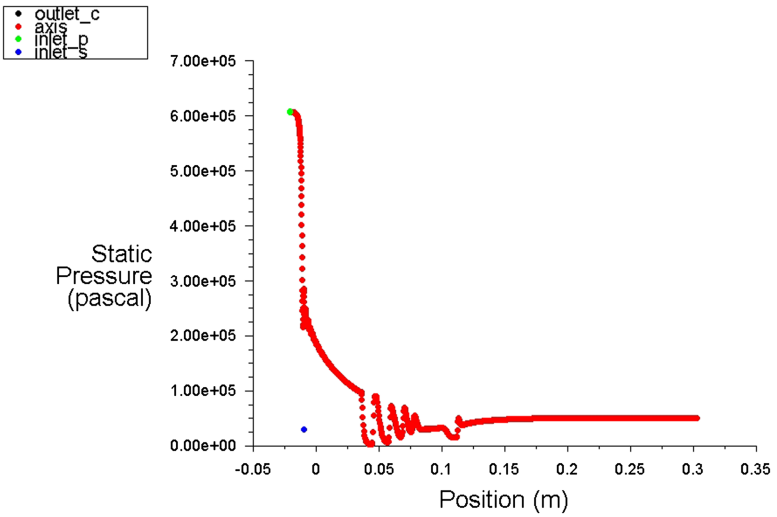

Figure 7. *Static pressure along the length of the ejector.*

5.1 Effect of variation of *Pp*

The effect of variation in *Pp* for two groups of ejectors and under adjustable spindle position (−25 mm) is shown in Figures 9 and 10. The mass flow rate in inlet primary ($\dot{m}_p$) increases, resulting in reducing of ω because growth in *Pp* leads to higher expansion of the primary flow from the primary nozzle exit. As presented in Figure 9, which consists of group C under *Pp* (6.0 bar), the ejector CB has the largest value of ω at about 0.43 from the rest of ejectors in this this group. The other ejectors (CA and CC) show the ω around 0.40 and 0.39, respectively.

Furthermore, Figure 10, which includes group A shows that the ejectors AB, AA and AC based on the same relationship have the same behaviour as group C. In these figures, the A_r of the six different ejectors is proportional to ω, the reason for this is when A_r increases, the flow in mixing stream increases as well and results in high ω at the choked state in the induced flow.

5.2 Effect of variation of *Pb*

Figures 11 and 12 show the effect of variation of *Pb* on ω for six different ejectors under a range of *Pp* (3–4.5 bar). Figure 11 illustrates the variation of *Pb* on ω for six different ejectors under *Pp* = 3.0 bar. It shows the highest to lowest values of entrainment ratios (ω) are 0.62, 0.59, 0.57, 0.57, 0.55 and 0.52 for ejectors CB, CA, CC, AB, AA and AC, respectively.

It can be seen that there are two groups of ejectors, group C with the highest values of ω and group A with the lowest values. In Figure 12, similar behaviour can be seen for all ejectors at *Pp* = 4.5 bar, but there is an increase in the range of back pressure. In addition, the ejector CB has the highest value 0.50 compared with the other ejectors at *Pp* = 4.5 bar. Moreover, the ejector AA displays the largest critical back pressure (*Pb*∗) amongst all ejectors. This latter ejector can be used for high *Pb* in various

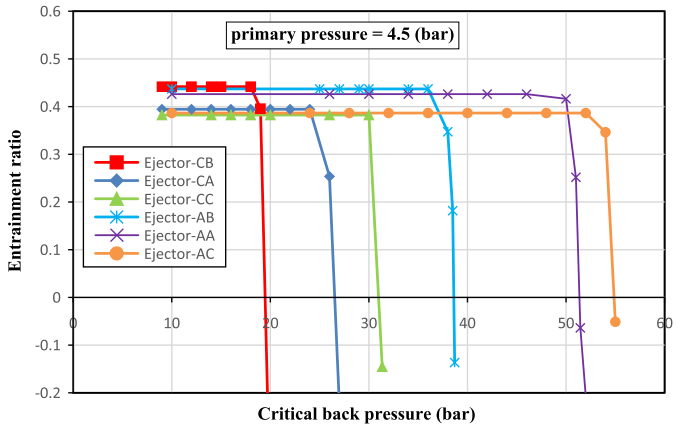

Figure 8. *Entrainment ratio vs. critical back pressure.*

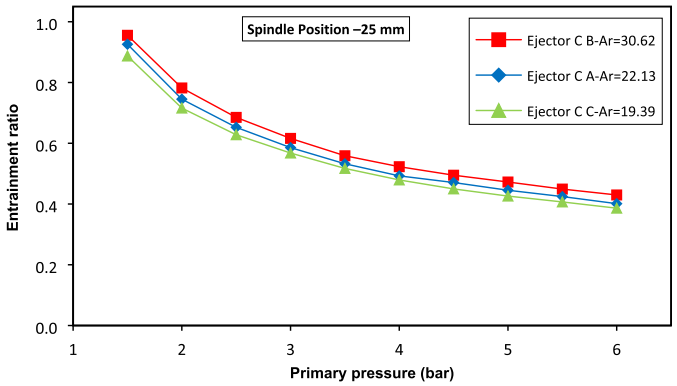

Figure 9. *Effect of variation of Pp on ω for group C of the ejector.*

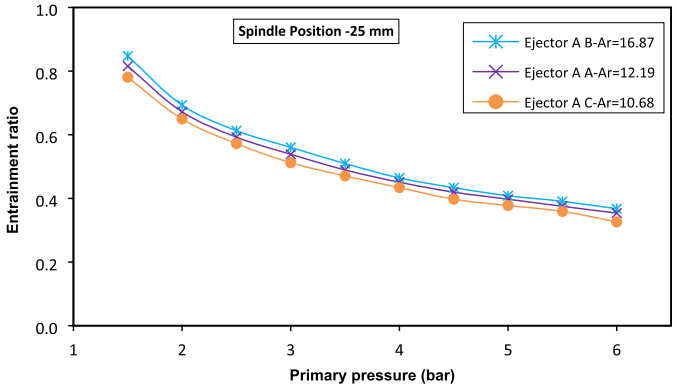

Figure 10. *Effect of variation of Pp on ω for group A of the ejector.*

applications, but the ejector CB can apply in high-performance applications.

Meanwhile, the relation between ω and $Pb*$ is also examined for six different ejectors. Figure 13 shows the relationship between the ω and the $Pb*$ at different Pp. As shown in this figure, it can be observed that ω decreases linearly as $Pb*$ increases and Pp increases from 3.0 to 4.5 bar. The highest value of ω and $Pb*$ are the same as shown in Figure 11 and Figure 12, wherein the two groups of ejectors have similar behaviour. it was found that the

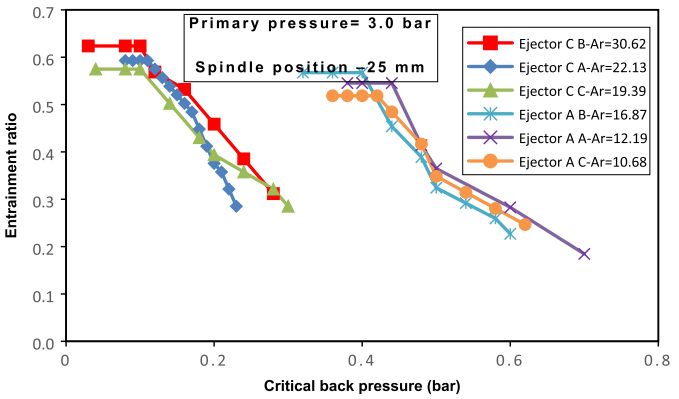

Figure 11. *Effect of variation of Pp on ω for six different ejectors at Pb = 3.0 bar.*

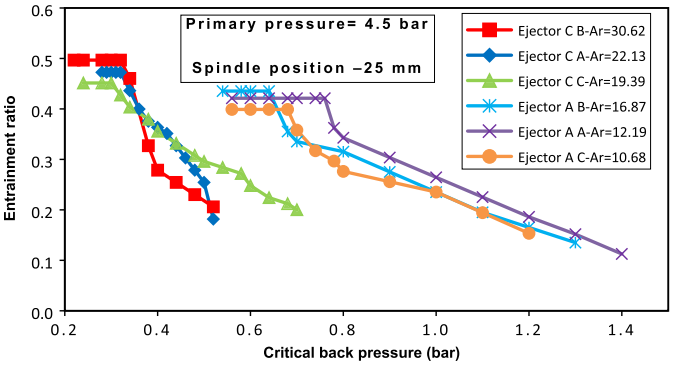

Figure 12. *Effect of variation of Pp on ω for six different ejectors at Pb = 4.5 bar.*

ejector CB has the highest value of the entrainment ratio ω and the lowest value belongs to the ejector AC. The reason for this is that the A_r of the ejector CB has the greatest value (30.62) and allows more mass of air to enter from the secondary flow port ($\dot{m}_s$) at sonic velocity (choking condition) into the mixed stream in the constant-area section. The ejector AA, which has $A_r = 12.19$ presents the highest value of $Pb*$ amongst ejectors, approximately 0.76 bar and entrainment ratio ω (0.42) at $Pp = 4.5$ bar. The rest of the ejectors have $Pb*$ approximately 0.32, 0.32, 0.32, 0.64 and 0.68 bar for CB, CA, CC, AB and AC, respectively.

5.3 Effect of variation of adjustable spindle position

Figure 14 shows the effect of variation of adjustable spindle positions on ω for ejector AA. The ω lines for ranges of Pp (1.5–6.0 bar) were carried out to compare different spindle positions. It is clear from the results that ω increases when the spindle increases under the same range of Pp (1.5–6.0 bar). For example, ω is 0.48, 0.60 and 0.84 as spindle positions are −5 mm, −15 mm and −25 mm at 1.5 bar. The reason for that is when the adjustable spindle position moves forward, the cross-section area of the primary nozzle decreases and leads to decreases in primary mass flow. Consequently, this results in reduced ω when the spindle moves backward from −5 mm to −25 mm. On the other hand, ω decreases nonlinearly when the spindle position and Pp increase.

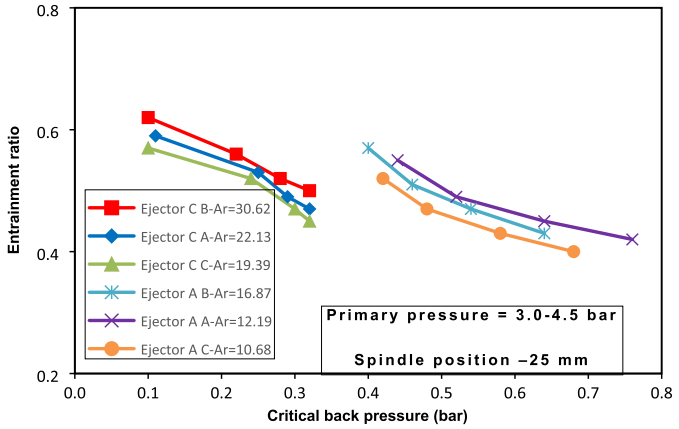

Figure 13. *Effect of Pb∗ on ω for the six ejectors.*

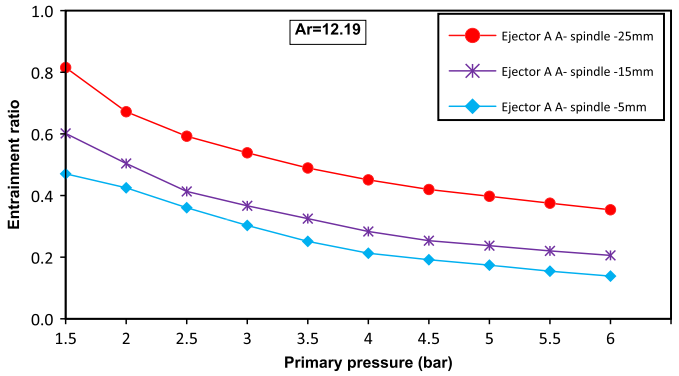

Figure 14. *Effect of variation of spindle positions on ω for ejector AA.*

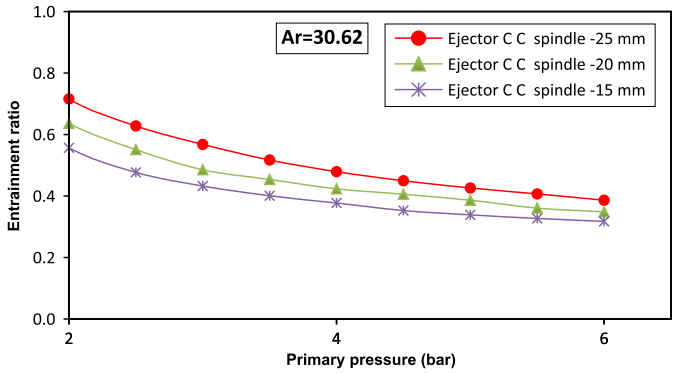

Figure 15. *Effect of variation of spindle positions on ω for ejector CC.*

It can be seen clearly that there is a reduction in ω for spindle positions in the range (1.5–3.0 bar) of *Pp*. After that, increasing *Pp* leads to a relatively small reduction in ω for spindle positions at *Pp* (3.0–6.0 bar), here, the entrainment ratios ω are 0.35, 0.21 and 0.14 at maximum *Pp* (6.0 bar) for positions −25 mm, −15 mm and −5 mm, respectively. While at 4.0 bar, the ratios are 0.21, 0.28 and 0.45 for spindle positions −5 mm, −15 mm and −25 mm, respectively.

With regard to ejector CC, it has the same tendency when the spindle position increases from −15 mm to −25 mm, as shown in Figure 15. It shows that the entrainment ratio (ω) under variation

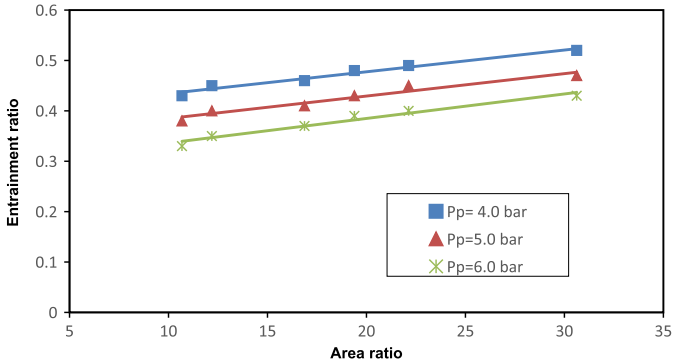

Figure 16. *Effect of variation of area ratio on ω under spindle position (−25 mm).*

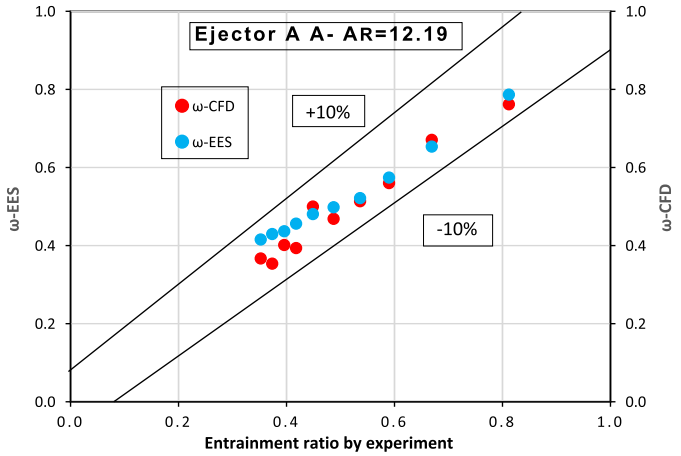

Figure 17. *Comparison of CFD and analytical results with experimental data.*

in *Pp* (1.5–6.0 bar) is larger than for ejector AA when using the same spindle position. At *Pp* = 6.0 bar, the maximal entrainment ratios (ω) obtained from this figure are 0.32, 0.35 and 0.39 for spindle positions −15 mm, −20 mm and −25 mm, respectively. While at *Pp* = 4.0 bar, the ratios are 0.38, 0.42 and 0.46 for spindle positions −15 mm, −20 mm and −25 mm, respectively. When the spindle position changes from 0 to 60% the ω and $\dot{m}_s$ rise but with less increment percentage in $\dot{m}_p$ [7, 10]. On the other hand, when the $\dot{m}_p$ increases through spindle position, the ω growths as the *Ps* is more than 1.0 bar but the ω drops when the *Ps* is less than 1.0 bar [9]. This leads us to the final explanation that the *Ps* has a significant effect on $\dot{m}_s$ if its value is lower than the design pressure, as shown in Figures 14 and 15.

5.4 Effect of variation of A_r

Figure 16 shows the effect of variation of A_r on ω, the ω lines for ranges of *Pp* (4.0–6.0 bar) were carried out to compare under fixed spindle position (−25 mm). The ω increases when A_r increases under the same *Pp*. For example, ω at *Pp* = 4.0 bar is 0.43, 0.45, 0.46, 0.48, 0.49 and 0.52 for ejectors AC, AA, AB, CC, CA and CB, respectively. While it is 0.33, 0.35, 0.37, 0.39, 0.4 and 0.43 for ejectors AC, AA, AB, CC, CA and CB, respectively, when

Pp = 6.0 bar. When *Pp* = 5.0 bar, the ω values are between the mentioned values for *Pp* = 4.0 bar and *Pp* = 6.0 bar. It can be concluded that ω decreases as *Pp* increases despite increasing A_r. This is because as the Pp increases, primary flow increases and leads to restrict ed more secondary flow to enter the mixing area and resulted in decreasing in (ω) when fixed A_r is used. However, (ω) will rise despite rising *Pp*, because more secondary flow will enter by enlarging the hypotheses area in the mixing region when the ejector is operating at *Pb* below the critical value.

5.5 Comparison of CFD and analytical results and experimental data

The comparison of analytical, CFD and experimental for ejector AA is shown in Figure 17. The relative errors for the experiment were ± 10% and ± 8% for the entrainment ratio calculated from EES (ω-EES) and the entrainment ratio calculated from CFD (ω-CFD). The CFD and EES models confirmed the experimental results of the ejector AA, therefore, the results obtained from CFD simulation verify the results calculated from the analytical technique (EES) and the experimental results.

6 CONCLUSION

In the present study, tests were carried out on six different ejectors to investigate primary pressure (*Pp*) effect on entrainment ratio (ω) by changing the spindle position from 0 to −25 mm. Furthermore, the back pressure (*Pb*) effect on ω under variation of *Pp* and spindle position was studied. Two groups of ejectors (each group includes three ejectors) based on the nozzle type were used in this study. Air is the working fluid used in all types of ejectors with range 1.5–6.0 bar, which is supplied from an air compressor. The main results can be summarized as below:

- The results showed that the ejector AA is more appropriate than the others for the highest values of *Pp*, while the ejector CB is more suitable for highest ω from the rest of ejectors. In fact, the ω is good predicted based on different geometries and operating conditions. Moreover, the maximum relative error ranges between 8% and 10%.
- The area ratio (A_r) is important for the design of the ejector. To get a better performance, the ejector should be designed with larger A_r. In addition, the ejector designed with smaller A_r will give the larger range of *Pb*.
- Furthermore, the secondary pressure (*Ps)* is very important to obtain a good result if its value is equal to the design value. Finally, the previous considerations of the ejector component can lead to use it widely with other working fluids in heating, ventilation, and air conditioning (HVAC) and combined cooling, heating and power (CCHP).

ACKNOWLEDGEMENTS

We should like to thank the financial contribution of Innovate UK for supporting the research project.

REFERENCES

[1] Abdulateef JM, Sopian K, Alghoul MA, Sulaiman MY. Review on solar-driven ejector refrigeration technologies. *Renew Sustain Energy Rev* 2009;**13**:1338–49 https://doi.org/10.1016/j.rser.2008.08.012.

[2] Varga S, Oliveira AC, Ma X *et al.* Experimental and numerical analysis of a variable area ratio steam ejector. *Int J Refrig* 2011;**34**:1668–75 https://doi.org/10.1016/j.ijrefrig.2010.12.020.

[3] Chandra VV, Ahmed MR. Experimental and computational studies on a steam jet refrigeration system with constant area and variable area ejectors. *Energ Conver Manage* 2014;**79**:377–86 https://doi.org/10.1016/j.enconman.2013.12.035.

[4] Varga S, Lebre PMS, Oliveira AC. CFD study of a variable area ratio ejector using R600a and R152a refrigerants. *Int J Refrig* 2013;**36**:157–65 https://doi.org/10.1016/j.ijrefrig.2012.10.016.

[5] Zhang B, Song X, Lv J, Zuo J. Study on the key ejector structures of the waste heat-driven ejector air conditioning system with R236fa as working fluid. *Energ Buildings* 2012;**49**:209–15 https://doi.org/10.1016/j.enbuild.2012.02.009.

[6] Zhang H, Wang L, Yan J *et al.* Performance investigation of a novel EEV-based ejector for refrigerator-freezers. *Appl Therm Eng* 2017;**121**:336–43 https://doi.org/10.1016/j.applthermaleng.2017.04.081 .

[7] Lin C, Cai W, Li Y *et al.* The characteristics of pressure recovery in an adjustable ejector multi-evaporator refrigeration system. *Energy* 2012;**46**:148–55 https://doi.org/10.1016/j.energy.2012.09.007 .

[8] Yen RH, Huang BJ, Chen CY *et al.* Performance optimization for a variable throat ejector in a solar refrigeration system. *Int J Refrig* 2013;**36**:1512–20 https://doi.org/10.1016/j.ijrefrig.2013.04.005.

[9] Lin C, Cai W, Li Y *et al.* Numerical investigation of geometry parameters for pressure recovery of an adjustable ejector in multi-evaporator refrigeration system. *Appl Therm Eng* 2013;**61**:649–56 https://doi.org/10.1016/j.applthermaleng.2013.08.033.

[10] Hou W, Wang L, Yan J *et al.* Simulation on the performance of ejector in a parallel hybrid ejector-based refrigerator-freezer cooling cycle. *Energ Conver Manage* 2017;**143**:440–7 https://doi.org/10.1016/j.enconman.2017.04.030.

[11] Huang BJ, Chang JM. Empirical correlation for ejector design. *Int J Refrig* 1999;**22**:379–88 https://doi.org/10.1016/S0140-7007(99)00002-X.

[12] Kumar V, Singhal G, Subbarao PMV. Study of supersonic flow in a constant rate of momentum change (CRMC) ejector with frictional effects. *Appl Therm Eng* 2013;**60**:61–71 https://doi.org/10.1016/j.applthermaleng.2013.06.045.

[13] Hemidi A, Henry F, Leclaire S *et al.* CFD analysis of a supersonic air ejector. Part I: Experimental validation of single-phase and two-phase operation. *Appl Therm Eng* 2009a;**29**:1523–31 https://doi.org/10.1016/j.applthermaleng.2008.07.003.

[14] Hemidi A, Henry F, Leclaire S *et al.* CFD analysis of a supersonic air ejector. Part II: Relation between global operation and local flow features. *Appl Therm Eng* 2009b;**29**:2990–8 https://doi.org/10.1016/j.applthermaleng.2009.03.019.

[15] Mazzelli F, Little AB, Garimella S, Bartosiewicz Y. Computational and experimental analysis of supersonic air ejector: Turbulence modeling and assessment of 3D effects. *Int J Heat Fluid Fl* 2015;**56**:305–16 https://doi.org/10.1016/j.ijheatfluidflow.2015.08.003.

[16] Eames IW. A new prescription for the design of supersonic jet-pumps: The constant rate of momentum change method. *Appl Therm Eng* 2002;**22**:121–31 https://doi.org/10.1016/S1359-4311(01)00079-5.

[17] Besagni G, Inzoli F. Computational fluid-dynamics modeling of supersonic ejectors: Screening of turbulence modeling approaches. *Appl Therm Eng* 2017;**117**:122–44 https://doi.org/10.1016/j.applthermaleng.2017.02.011.

[18] Keenan J, Neumann E, Lustwerk F. An investigation of ejector design by analysis and experiment. *ASME J Appl Mech*, *J Appl Mech* 1950;**72**, **17**:299, 299–309.

[19] Eames I, Aphornratana S, Haider H. A theoretical and experimental study of a small-scale steam jet refrigerator. *Int J Refrig* 1995;**18**:378–86 https://doi.org/10.1016/0140-7007(95)98160-M.

[20] Khalil A, Fatouh M, Elgendy E. Ejector design and theoretical study of R134a ejector refrigeration cycle. *Int J Refrig* 2011;**34**:1684–98.

[21] Chen X, Zhou Y, Yu J. A theoretical study of an innovative ejector enhanced vapor compression heat pump cycle for water heating application. *Energ Buildings* 2011;**43**:3331–6.

[22] Chen W, Liu M, Chong D *et al.* A 1D model to predict ejector performance at critical and sub-critical operational regimes. *Int J Refrig* 2013;**36**:1750–61 https://doi.org/10.1016/j.ijrefrig.2013.04.009.

[23] Huang B. A 1-D analysis of ejector. *Int J Refrig* 1999;**22**:354–64 https://doi.org/10.1016/S0140-7007(99)00004-3.

[24] Godefroy J, Boukhanouf R, Riffat S. Design, testing and mathematical modelling of a small-scale CHP and cooling system (small CHP-ejector trigeneration). *Appl Therm Eng* 2007;**27**:68–77 https://doi.org/10.1016/j.applthermaleng.2006.04.029.